PHYSICAL REVIEW D **93,** 084051 (2016)

Gravitational lensing by gravastars

Tomohiro Kubo and Nobuyuki Sakai*

Graduate School of Science and Engineering, Yamaguchi University, Yamaguchi 753-8512, Japan

(Received 8 March 2016; published 29 April 2016)

As a possible method to detect gravastars (gravitational-vacuum-star), which was originally proposed by Mazur and Mottola, we study their gravitational lensing effects. Specifically, we adopt a spherical thin-shell model of a gravastar developed by Visser and Wiltshire, which connects interior de Sitter geometry and exterior Schwarzschild geometry, and assume that its surface is optically transparent. We calculate the image of a companion which rotates around the gravastar; we find that some characteristic images appear, depending on whether the gravastar possess unstable circular orbits of photons (Model 1) or not (Model 2). For Model 2, we calculate the total luminosity change, which is called microlensing effects; the maximal luminosity could be considerably larger than the black hole with the same mass.

DOI: 10.1103/PhysRevD.93.084051

I. INTRODCUTION

Gravastars (*gravitational vacuum stars*) were originally proposed by Mazur and Mottola [1] as a new final state of gravitational collapse of stars, that is, an alternative to black holes: they are spherically symmetric supercompact objects which mimic black holes. In their model an interior de Sitter region and an exterior Schwarzschild background are connected by a shell of stiff matter ($p = \rho$) so that singularity in Schwarzschild spacetime is removed. Although their formation process is unclear, the idea is fascinating because it could solve two fundamental problems of black holes: the singularity problem and information loss paradox.

Since their original proposal, a number of models of gravastars have been studied. Cattoen *et al.* [2] showed that gravastars cannot be perfect fluids and hence anisotropic pressure should be included. Therefore, the subsequent models are classified into two types: one is continuous matter with anisotropic pressure [2,3] and the other is an infinitely thin shell [4–9]. The original thin-shell model of a gravastar was developed by Visser and Wiltshire (VW) [4], using Israel's junction conditions [10]. In their model there are not only static solutions but also stably oscillating solutions; the latter class was studied carefully by Rocha *et al.* [5]. Then, many extensive models have been discussed: generalized equation of state [6], radiating shell [7], including dark energy [8], and including electromagnetic field [9].

If gravastars exist in the Universe, how can we identify them by observations? Chirenti and Rezzolla [11] considered a question of how to tell a gravastar from a black hole. They studied axial-perturbations on gravastars and found that their quasinormal modes of gravitational waves differ from those of black holes. Later more general perturbations were analyzed by Pani *et al.* [12] Broderick and Narayan [13] argued that, if observed black hole candidates with matter accretion were gravastars, they should heat up and emit radiation. With this thermal process they discussed observational constraints on gravastar models. Harko *et al.* [14] considered accretion disks around slowly rotating gravastars and argued that their electromagnetic properties can distinguish a gravastar from a black hole.

Recently Sakai, Saida and Tamaki [15] proposed a new method to distinguish gravastars from black holes by electromagnetic observations. They investigated the optical images of the gravastars possessing unstable circular orbits of photons, assuming its optically transparent surface and two types of optical sources behind a gravastar: an infinite optical plane and a companion star.

In this paper we focus on the latter case: assuming its optically transparent surface, we investigate the image and luminosity change of a companion rotating a gravastar in more depth to answer the following questions.

(i) What is the image of the companion like when it is in front of the gravastar?
(ii) What is the image of the companion like if the lens gravastar is slightly larger and does not possess unstable circular orbits of photons?
(iii) How does the total luminosity change when the companion passes through the gravastar?

The last question is the most important because it is more realistic to observe the total luminosity (i.e., microlensing effects) than to observe the shape of the lensed image.

The present analysis is also applicable to the study of boson stars [16] and other soliton stars composed of scalar fields or gauge fields. Because such soliton stars are optically transparent, we expect that they have similar optical natures.

This paper is organized as follows. In Sec. II, we review thin-shell models of a gravastar used in Ref. [15] and discuss null geodesics for the two models: one possesses an unstable circular orbits of photons and the other is not.

*nsakai@yamaguchi-u.ac.jp

In Sec. III, we solve null geodesic equations numerically to obtain the images of optical source around gravastar for the two models; we also calculate the time-variation of the total luminosity. Section IV is devoted to concluding remarks.

II. THIN SHELL MODEL AND NULL GEODESICS

A. Thin shell model

To begin with, we review thin-shell models of a gravastar developed by Visser and Wiltshire [4], which was adopted in Ref. [15]. The inside is a part of de Sitter spacetime,

$$ds^2 = -A_-dt^2 + \frac{dr_-^2}{A_-} + r_-^2(d\theta^2 + \sin^2\theta d\phi^2), \tag{2.1}$$

$$\text{with} \quad A_-(r_-) \equiv 1 - H^2 r_-^2, \tag{2.2}$$

and the outside is a part of Schwarzschild spacetime,

$$ds^2 = -A_+dt^2 + \frac{dr_+^2}{A_+} + r_+^2(d\theta^2 + \sin^2\theta d\phi^2), \tag{2.3}$$

$$\text{with} \quad A_+(r_+) \equiv 1 - \frac{r_g}{r_+}, \tag{2.4}$$

where r_g is a gravitational radius. We have denoted the field variable on the outside (inside) by superscripts or subscripts $+(-)$. To describe the geometry in vicinity of the boundary hypersurface Σ, we introduce a Gaussian normal coordinate system,

$$\begin{aligned} ds^2 &= dn^2 + \gamma_{ij}^{\pm} dx^i dx^j \\ &= dn^2 - N_{\pm}(n,\tau)^2 d\tau^2 \\ &\quad + r_{\pm}(n,\tau)^2(d\theta^2 + \sin^2\theta d\phi^2), \end{aligned} \tag{2.5}$$

in which $n = 0$ corresponds to Σ. N is normalized by $N_{\pm}(0,\tau) = 1$ so that τ implies the proper time of Σ. We suppose that Σ contents infinitesimally thin matter,

$$S_j^i \equiv \int_{-0}^{+0} T_j^i dn = \mathrm{diag}(-\sigma, \varpi, \varpi), \tag{2.6}$$

where σ and ϖ are the surface energy density and the surface pressure, respectively. Following Visser and Wiltshire [4], we assume $2+1$ dimensional stiff matter,

$$\varpi = \sigma. \tag{2.7}$$

What we are looking for is static and stable solutions of a gravastar. To find the solutions which are stable against spherical perturbations, we derive the equations of motion of the shell.

Following Israel's formalism [10,17], we can obtain the junction conditions at Σ as follows. The metric continuity $\gamma_{ij}^+ = \gamma_{ij}^-$ implies

$$R = r_+ = r_-, \tag{2.8}$$

$$d\tau^2 = A_+dt_+^2 - \frac{dr_+^2}{A_+} = A_-dt_-^2 - \frac{dr_-^2}{A_-}. \tag{2.9}$$

The other junction conditions are reduced to the two equations. One is

$$\beta_- - \beta_+ = 4\pi G\sigma R, \tag{2.10}$$

where

$$\begin{aligned} \beta_{\pm} &\equiv \frac{\partial r_{\pm}}{\partial n} = \varepsilon_{\pm}\sqrt{\left(\frac{dR}{d\tau}\right)^2 + A_{\pm}}, \\ \varepsilon_{\pm} &\equiv \mathrm{sign}\frac{\partial r_{\pm}}{\partial n}. \end{aligned} \tag{2.11}$$

In a spacetime without Schwarzschild horizon nor de Sitter horizon, $\varepsilon_{\pm} = +1$ because the areal radius $r_{\pm}$ always increases as n increases. The other equation is

$$\frac{d}{d\tau}(\sigma R^2) + \varpi\frac{d}{d\tau}(R^2) = 0. \tag{2.12}$$

For stiff matter (2.7), we find

$$\sigma R^4 = \text{const.} \tag{2.13}$$

Introducing dimensionless quantities,

$$\tilde{R} \equiv \frac{R}{r_g}, \qquad \tilde{\tau} \equiv \frac{\tau}{r_g} \tag{2.14}$$

$$h \equiv r_g H, \qquad s \equiv \frac{4\pi G\sigma R^4}{r_g^3} = \text{const}, \tag{2.15}$$

we rewrite (2.10) as

$$\left(\frac{d\tilde{R}}{d\tilde{\tau}}\right)^2 + U(\tilde{R}) = 0. \tag{2.16}$$

$$\begin{aligned} U(\tilde{R}) \equiv 1 &- \frac{h^2\tilde{R}^2}{2} - \frac{1}{2\tilde{R}} - \frac{s^2}{4\tilde{R}^6} \\ &- \frac{\tilde{R}^6}{4s^2}\left(h^2\tilde{R}^2 - \frac{1}{\tilde{R}}\right)^2. \end{aligned} \tag{2.17}$$

We have to solve $U(\tilde{R}) = 0$ and $U'(\tilde{R}) = 0$ to obtain static and stable solutions. This condition gives a constraint on the three parameters h, s, and $\tilde{R}$. We survey static and stable solutions and show their parameters s, $\tilde{R}$ as a function of h in Fig. 1. In the following analysis we adopt the two cases, which are denoted by the bigger dots in Fig. 1.

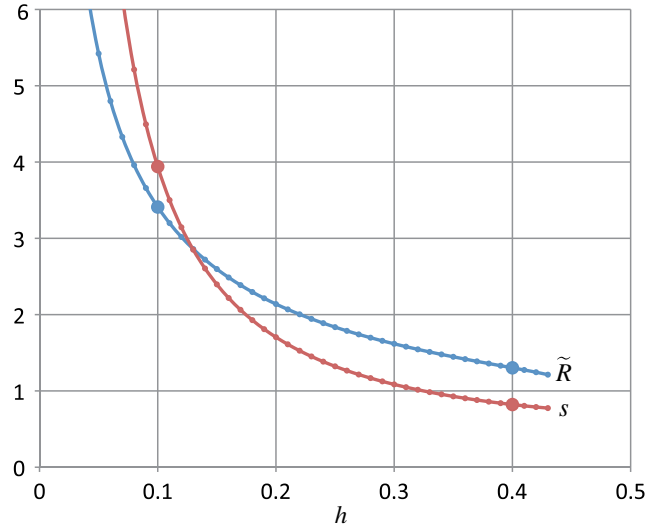

FIG. 1. Parameters s and $\tilde{R}$ as a function of h, when $U(\tilde{R})$ has a local minimum on $U(\tilde{R}) = 0$ as shown in Fig. 1. Only these parameter values allow for static and stable gravastar solutions. h has an upper limit, $h_{\max} \approx 0.43$. The large dots denote the two cases, $h = 0.1$, $\tilde{R} = 1.303$ (Model 1) and $h = 0.4$, $\tilde{R} = 3.410$ (Model 2), which we analyze in the following.

(i) *Model 1*: $h = 0.1$, $\tilde{R} = 1.303$. Because $R < 1.5r_g$, unstable circular orbits of photons are existent.
(ii) *Model 2*: $h = 0.1$, $\tilde{R} = 3.410$. Because $R > 1.5r_g$, unstable circular orbits of photons are nonexistent.

B. Null geodesic equations

Next, we derive null geodesic equations with boundary conditions for the static gravastar spacetime. The null geodesic equations are

$$\frac{dk^\mu}{d\lambda} + \Gamma^\mu_{\nu\rho} k^\nu k^\rho = 0, \quad \text{with} \quad k_\mu k^\mu = 0. \tag{2.18}$$

The geodesics in the $\theta = \pi/2$ plane for the outside $(+)$ and the inside $(-)$ are given by

$$\frac{d}{d\lambda_\pm}(A_\pm k^t_\pm) = 0, \qquad \frac{d}{d\lambda_\pm}(r^2_\pm k^\varphi_\pm) = 0, \tag{2.19}$$

$$\frac{1}{\sqrt{A_\pm}} \frac{d}{d\lambda_\pm}\left(\frac{k^r_\pm}{\sqrt{A_\pm}}\right) + \frac{dA_\pm}{dr_\pm}\frac{(k^t_\pm)^2}{2} - r_\pm (k^\varphi_\pm)^2 = 0, \tag{2.20}$$

$$-A_\pm (k^t_\pm)^2 + \frac{(k^r_\pm)^2}{A_\pm} + r^2_\pm (k^\varphi_\pm)^2 = 0. \tag{2.21}$$

Because Eq. (2.20) is also derived by (2.19) and (2.21), we do not have to solve it. Equations (2.19) are integrated as

$$A_\pm k^t_\pm = \text{const} \equiv E_\pm, \qquad r^2_\pm k^\varphi_\pm = \text{const} \equiv L_\pm, \tag{2.22}$$

and then (2.21) becomes

$$(k^r_\pm)^2 + \frac{A_\pm L^2_\pm}{r^2_\pm} = E^2_\pm. \tag{2.23}$$

It follows from (2.22) and (2.23) that

$$\frac{dr_\pm}{d\varphi} = \frac{k^r_\pm}{k^\varphi_\pm} = \frac{r^2_\pm k^r_\pm}{L_\pm} = \pm r_\pm \sqrt{\left(\frac{E_\pm r_\pm}{L_\pm}\right)^2 - A_\pm}, \tag{2.24}$$

which gives null geodesics in the exterior and interior regions of the gravastar.

The equation for the interior region in (2.24) is integrated as

$$r_- = r_m \sec(\varphi - \varphi_m), \qquad r_m \equiv \left(\frac{E^2_-}{L^2_-} + H^2\right)^{-\frac{1}{2}}, \tag{2.25}$$

where φ_m is an integral constant. Since a black hole horizon does not exist and the surface of the gravastar is transparent in our situation, any incident light ray to the gravastar has to penetrate the gravastar, as we will show in Fig. 3. Therefore, there are two crossing points of the penetrating null geodesic with the surface of gravastar Σ. Let φ_1 and $\varphi_2 (\varphi_1 < \varphi_2)$ denote the φ-coordinate values of those two crossing points, they are determined by

$$\varphi_m = \varphi_1 + \arccos\frac{r_m}{R} = \varphi_2 - \arccos\frac{r_m}{R}. \tag{2.26}$$

On the other hand, the equation for the exterior region in (2.24) cannot be integrated analytically. However, the asymptotic solution at $r \to \infty$ is obtained by putting $A_+ \to 1$:

$$r_+ = \frac{L_+}{E_+}\sec(\varphi - \varphi_c), \tag{2.27}$$

where φ_c is an integral constant.

Next, we discuss the boundary conditions of k^μ at Σ. In the case of a static gravastar, $R = \text{const}$, the relation between the Gaussian normal coordinates (2.5) and the outer/inner coordinates (2.1) and (2.3) is given by

$$\begin{aligned} d\tau^2 &= A_+ dt^2_+ = A_- dt^2_-, \\ R^2 d\varphi^2 &= r^2_+ d\varphi^2 = r^2_- d\varphi^2. \end{aligned} \tag{2.28}$$

Then we find

$$\sqrt{A_+}\, k^t_+ = \sqrt{A_-}\, k^t_-, \qquad k^\varphi_+ = k^\varphi_-. \tag{2.29}$$

With the help of the null condition (2.21), we also obtain

$$\frac{k^r_+}{\sqrt{A_+}} = \frac{k^r_-}{\sqrt{A_-}}. \tag{2.30}$$

The relations among the integration constants are given by (2.8), (2.22) and (2.29),

$$L_+ = L_-, \qquad \frac{E_+}{\sqrt{A_+}} = \frac{E_-}{\sqrt{A_-}}. \tag{2.31}$$

Hereafter we denote L_+ and L_- simply by L because they are identical.

To make a qualitative discussion on photon trajectories, it is convenient to introduce the effective potential as follows. Equation (2.23) is rewritten as

$$\left(\frac{dr_\pm}{d\lambda_\pm}\right)^2 + \frac{L^2 A_\pm}{r_\pm^2} = E_\pm^2. \tag{2.32}$$

To discuss the dynamics with a continuous "potential" by analogy with the Newtonian mechanics, we introduce unified variables as

$$r = r_- \quad \text{and} \quad \lambda = \sqrt{\frac{A_-(R)}{A_+(R)}}\lambda_- \quad \text{(inside)},$$
$$r = r_+ \quad \text{and} \quad \lambda = \lambda_+ \quad \text{(outside)}, \tag{2.33}$$

and define the effective potential as

$$V(r<R) = \frac{L^2 A_-}{r^2}\frac{A_+(R)}{A_-(R)} = L^2\frac{A_+(R)}{A_-(R)}\left(\frac{1}{r^2} - H^2\right),$$
$$V(r>R) = \frac{L^2 A_+}{r^2} = L^2\left(\frac{1}{r^2} - \frac{r_g}{r^3}\right). \tag{2.34}$$

Then we obtain the continuous equation of motion,

$$\left(\frac{dr}{d\lambda}\right)^2 + V(r) = E_+^2. \tag{2.35}$$

Figure 2 shows $V(r)$ for the two models. Model 1 represents the case where both stable and unstable circular orbits of photons, while Model 2 represents the case where no circular orbits of photons.

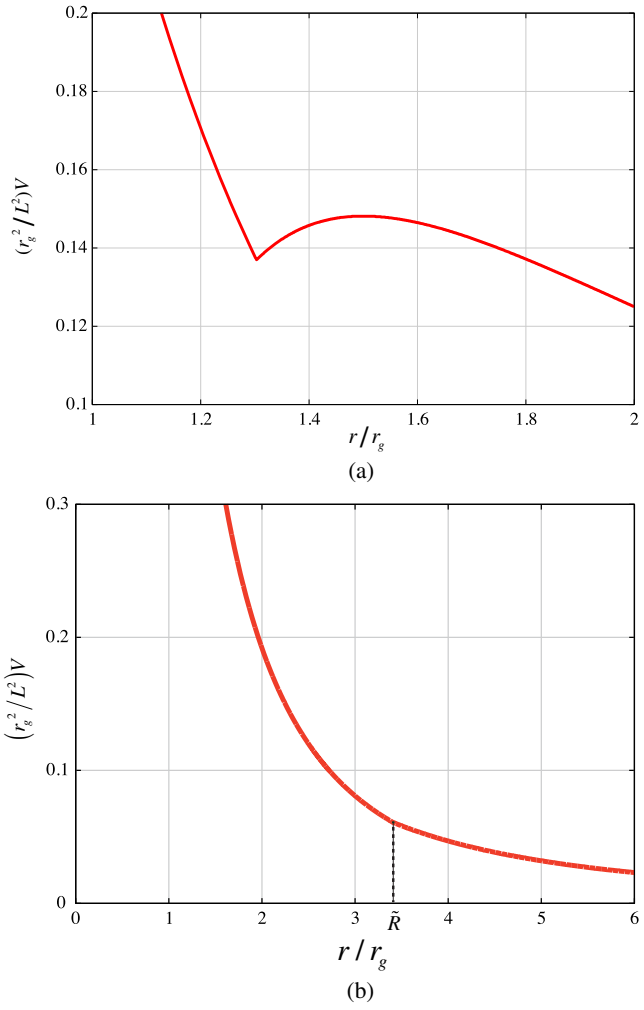

FIG. 2. Graphs of the effective potential of null geodesics, $V(\tilde{R})$. (a) Model 1 has both stable and unstable circular orbits of photons. (b) Model 2 has no circular orbits of photons.

III. GRAVITATIONAL LENS BY GRAVASTARS

A. Basics features of null geodesics

We review the basic features of null geodesics, which was discussed in Ref. [15]. We define the rectangular coordinates $(x, y, z) = (r\cos\varphi\sin\theta, r\sin\varphi\sin\theta, r\cos\theta)$. We suppose that the center of the gravastar is located at the origin and the observer at $(D_o, 0, 0)(\varphi = 0)$. Figure 3 shows the $z = 0(\theta = \pi/2)$ plane. If we make a coordinate rotation appropriately, any trajectory can be put on this plane. On this plane, we denote the intersection of the y-axis with the tangent to the ray at the observer by $y = \alpha$; we can interpret α as the apparent length from the gravastar's center or the impact parameter.

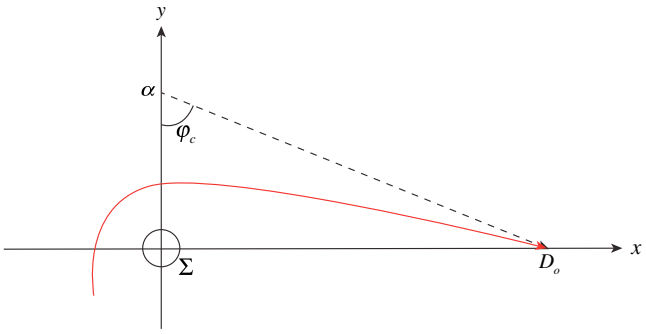

FIG. 3. The $z = 0$ plane in the 3-space $(x, y, z) = (r\cos\varphi\sin\theta, r\sin\varphi\sin\theta, r\cos\theta)$. The center of the gravastar is located at the origin and the observer at $(D_o, 0, 0)$. The intersection of the y-axis with the tangent to the ray at the observer is denoted by $(0, \alpha, 0)$. The integral constant φ_c corresponds to the angle indicated by this figure: $\tan\varphi_c = D_o/\alpha$.

In this rectangular coordinate system the asymptotic solution (2.27) is rewritten as

$$x\cos\varphi_c + y\sin\varphi_c = \frac{L}{E}, \tag{3.1}$$

where the x-intercept and the y-intercept are given by

$$D_o = \frac{L}{E}\sec\varphi_c, \qquad \alpha = \frac{L}{E}\mathrm{cosec}\varphi_c, \tag{3.2}$$

respectively. Recall that φ_c is an integral constant defined by (2.27). Because (3.2) indicates

$$\tan\varphi_c = \frac{D_o}{\alpha}, \tag{3.3}$$

we find that the integral constant φ_c corresponds to the angle indicated by Fig. 3.

Furthermore, taking the limit of $D_o \to \infty$, we obtain

$$\varphi_c \to \frac{\pi}{2}, \qquad \alpha \to \frac{L}{E}. \tag{3.4}$$

Therefore, if D_o is large enough, we can regard L/E as the apparent length from the center as well as the impact parameter. In the following analysis we put $D_o = 1000r_g$.

Figure 4 shows trajectories of photons which reach the observer for (a) Model 1 and (b) Model 2. In de Sitter region photons pass linearly. In Model 1 photons with $L/Er_g \approx 3\sqrt{3}/2$ twines around the unstable circular orbit. In Model 2 lensing effects are smaller than those in model 1; however, the amplification of luminosity becomes more important.

B. Gravitational lensing images

Next, supposing that a companion star rotates around a gravastar, we investigate its image caused by gravitational lens effects. Figure 5 shows the setting of our numerical analysis. We suppose the companion is rotating around the gravastar. We put the gravastar's center and the companion's center at the origin and on the $z = 0$-plane, respectively. We denote the distance between the companion's center and the gravastar's center by D_s and the radius of the companion by r_s. The angle δ is defined as the angle between the direction of the companion's center and the opposite direction to x-axis. The image $\vec{\alpha} = (\alpha_y, \alpha_z)$ is defined as the intersection of the $x = 0$ plane with the tangent to the ray at the observer.

Henceforth we discuss the two models separately.

(i) Model 1 ($h = 0.4$, $\tilde{R} = 1.303 < 1.5$).

We show the relation between the apparent position $\alpha = L/Er_g$ and the central angle δ in Fig. 6, which provides us all information about lensing effects. The peak sharp peak at $\alpha = 1.5\sqrt{3} \approx 2.5981$ corresponds to the geodesics which wind infinite times on the unstable circular orbits $r = 1.5r_g$, and diverges at $\alpha = 1.5\sqrt{3}$. While the photons with $\alpha > 1.5\sqrt{3}$ travel only in Schwarzschild background,

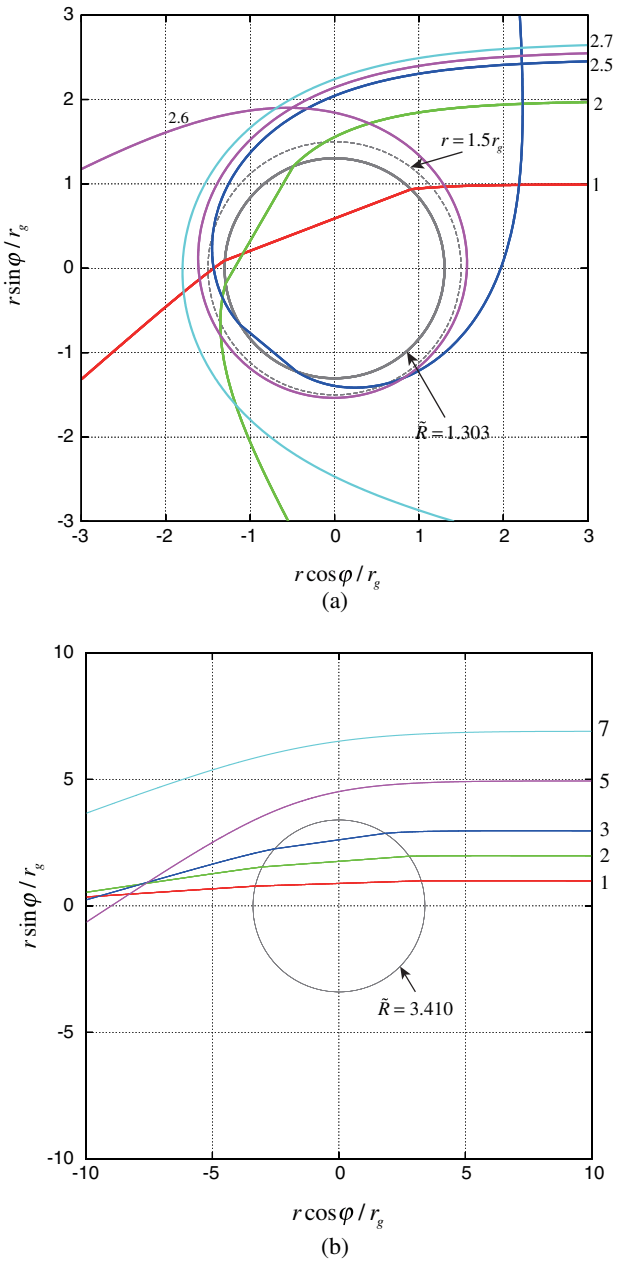

FIG. 4. Trajectories of photons which reach the observer for (a) Model 1 and (b) Model 2. The observer is located at $r = 1000r_g$, $\phi = 0$, the right side of the figure. In de Sitter region photons pass linearly. In Model 1 photons with $L/Er_g \approx 3\sqrt{3}/2$ twines around the unstable circular orbit. In Model 2 lensing effects are smaller than those in model 1; however, the amplification of luminosity becomes more important.

the photons with $\alpha < 1.5\sqrt{3}$ pass through the gravastar interior. In pure Schwarzschild spacetime only geodesics with $\alpha > 1.5\sqrt{3}$ exist.

Figure 7 shows the images of the companion projected onto the $x = 0$ plane when it is behind the gravastar ($\delta > 90°$), which was also discussed in Ref. [15]. The gravastar's center is fixed at the origin. We take $D_s = 10r_g$

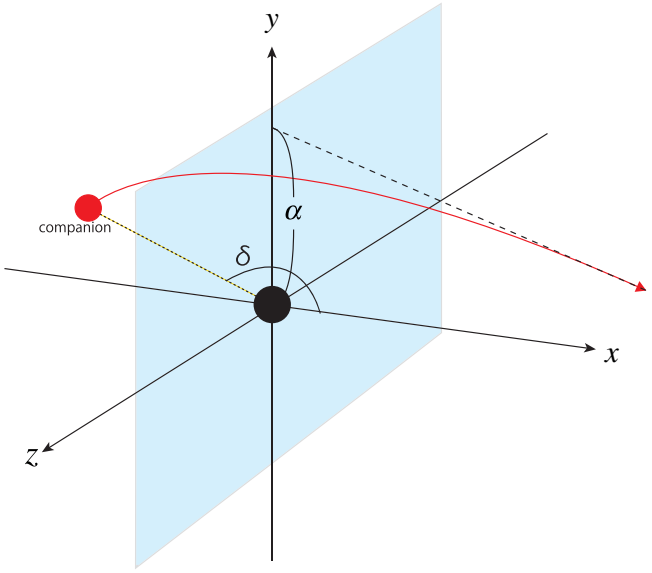

FIG. 5. Setting of our analysis of gravitational lens effects. We suppose a companion around a gravastar. We put the gravastar's center and the companion's center at the origin and on the $z = 0$-plane, respectively. We denote the distance between the companion's center and the gravastar's center by D_s and the radius of the companion by r_s. The angle δ is defined as the angle between the direction of the companion's center and the opposite direction to x-axis. The image $\vec{\alpha} = (\alpha_y, \alpha_z)$ is defined as the intersection of the $x = 0$ plane with the tangent to the ray at the observer.

and $r_s = 2r_g$. We display five snapshots when $\delta = 100°$, 135°, 150°, 168° and 170°. The red images correspond to geodesics which pass through the gravastar, while the blue ones to those which pass only through Schwarzschild

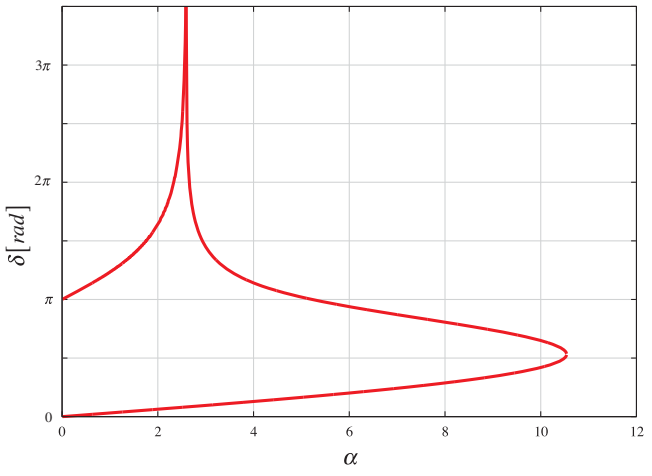

FIG. 6. Relation between the apparent position α and the central angle δ for Model 1 ($\tilde{R} < 1.5$). The sharp peak at $\alpha = 1.5\sqrt{3} \approx 2.5981$ corresponds to the geodesics which wind infinite times on the unstable circular orbit $r = 1.5r_g$, and diverges at $\alpha = 1.5\sqrt{3}$. While the photons with $\alpha > 1.5\sqrt{3}$ travel only in Schwarzschild background, the photons with $\alpha < 1.5\sqrt{3}$ pass through the gravastar interior.

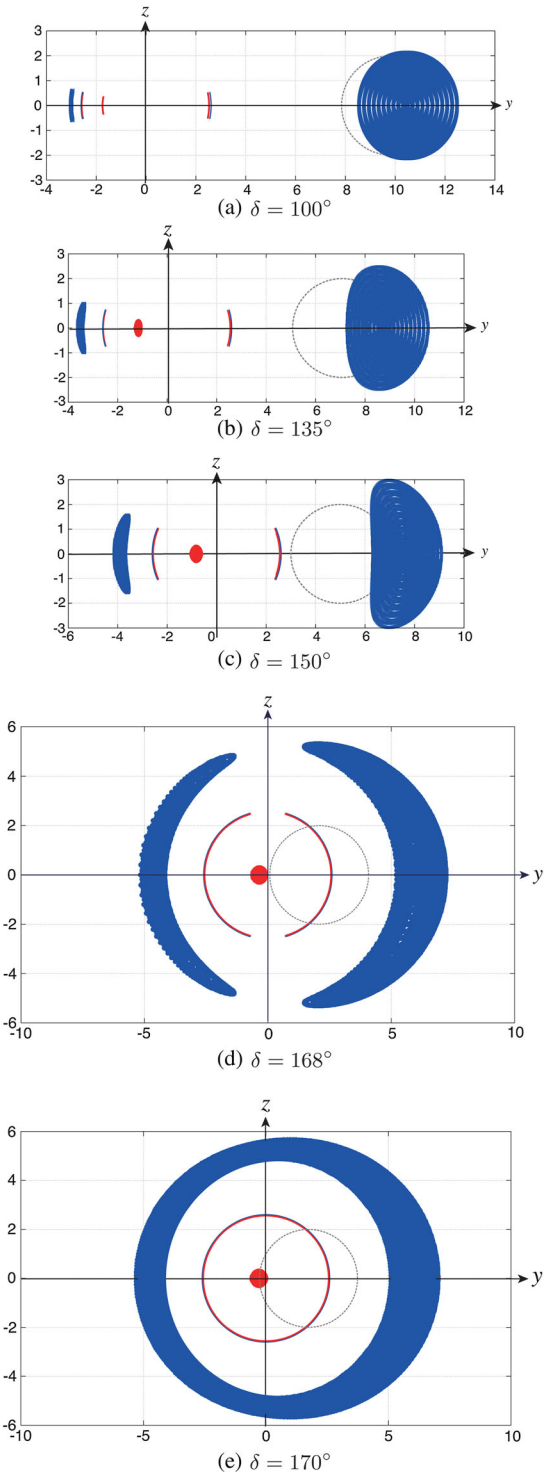

FIG. 7. Images of the companion for Model 1 when it is behind the gravastar ($\delta > 90°$). The gravastar's center is fixed at the origin. We choose $D_s = 10r_g$ and $r_s = 2r_g$. We display five snapshots when $\delta = 100°$, 135°, 150°, 168° and 170° in (a), (b), (c), (d) and (e), respectively. The red images correspond to geodesics which pass through the gravastar, while the blue ones to those which pass only through Schwarzschild background. The dotted circles indicate the image in the absence of the gravastar. We do not take account of light-dark contrast, which is generated by gravitational redshift of the photons.

background. The dotted circles indicate the image in the absence of the gravastar. Here we do not take account of light-dark contrast, which is generated by gravitational redshift of the photons. The characteristics of the gravastar are the red images: a disk in the center and arcs in the sides. Actually, there are infinite numbers of arcs between the red arc and the blue arc. As the companion moves, the central disk moves in the opposite direction. As δ increases, the arcs in both sides become longer, and finally they are combined into one image.

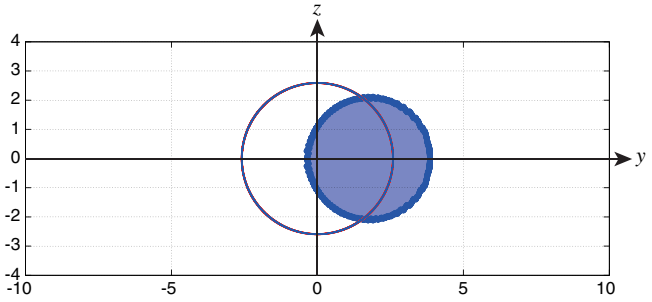

(a) $\delta = 10°$

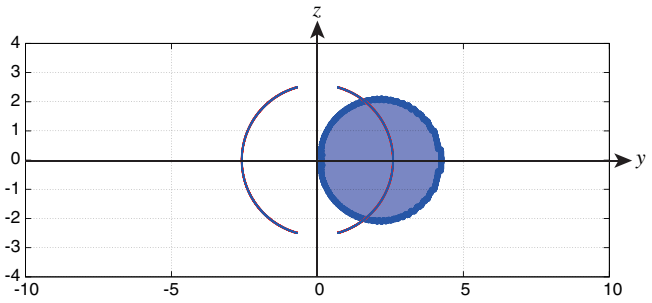

(b) $\delta = 12°$

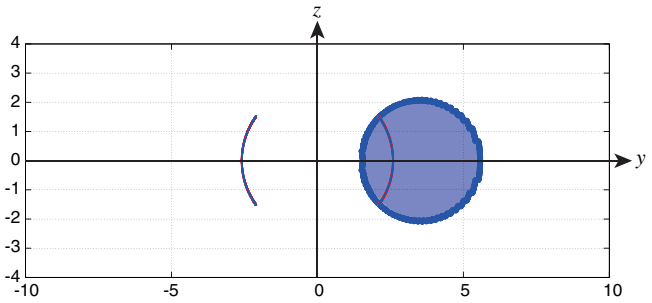

(c) $\delta = 20°$

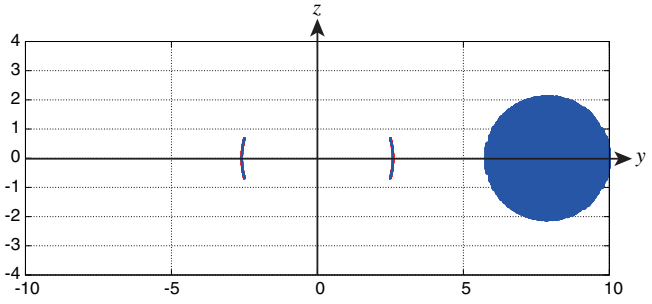

(d) $\delta = 50°$

FIG. 8. Images of the companion for Model 1 when it comes in front of the gravastar ($\delta > 90°$). We display four snapshots when $\delta = 10°$, 12°, 20° and 50° in (a), (b), (c) and (d), respectively. The disc is a "direct" image which is insignificantly affected by gravity. The rings and arcs correspond to photons which go around the gravastar.

Figure 8 shows the images for the same model when the companion comes in front of the gravastar ($\delta < 90°$). We display four snapshots when $\delta = 10°$, 12°, 20° and 50°. The blue disc is a "direct" image which is insignificantly affected by gravity. The rings and arcs correspond to photons which go around the gravastar. When $\delta \lessapprox 12°$, one disc and many rings appear; as δ increases, the rings are broken into arcs.

(ii) Model 2 ($h = 0.1, \tilde{R} = 3.410 > 1.5$).

Next, we consider Model 2, which does not possess unstable circular orbits of photons. Although lensing effects in Model 2 are smaller than those in Model 1, the amplification of luminosity would be more important and observable.

Figure 9 shows the relation between the apparent position $\alpha = L/Er_g$ and the central angle δ. The small peak corresponds to the geodesics which pass the surface of the gravastar.

Figure 10 shows the images of the companion for Model 2. Again we choose $D_s = 10r_g$ and $r_s = 2r_g$. We display six snapshots when $\delta = 130°$, 150°, 160°, 167°, 170° and 175°. Although lensing effects are weaker than those in Model 1, we find new features as follows.

(i) When $\delta \lessapprox 160°$, only blue-colored images, which denote geodesics which pass only through Schwarzschild background, appear. The number of images are only one or two, contrary to Model 1, where infinite numbers of arcs appear.

(ii) When $\delta \gtrapprox 167°$, one or two red images, which denote geodesics pass through the gravastar, also appear.

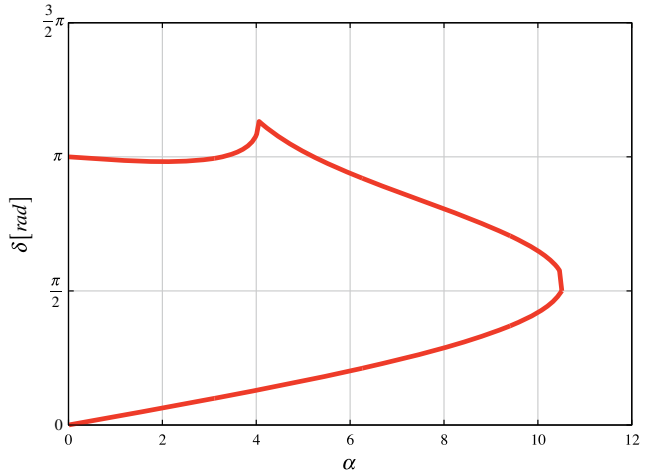

FIG. 9. Relation between the impact parameter α and the companion angle δ for Model 2 ($\tilde{R} > 1.5$). The small peak corresponds to the geodesics which pass the surface of the gravastar.

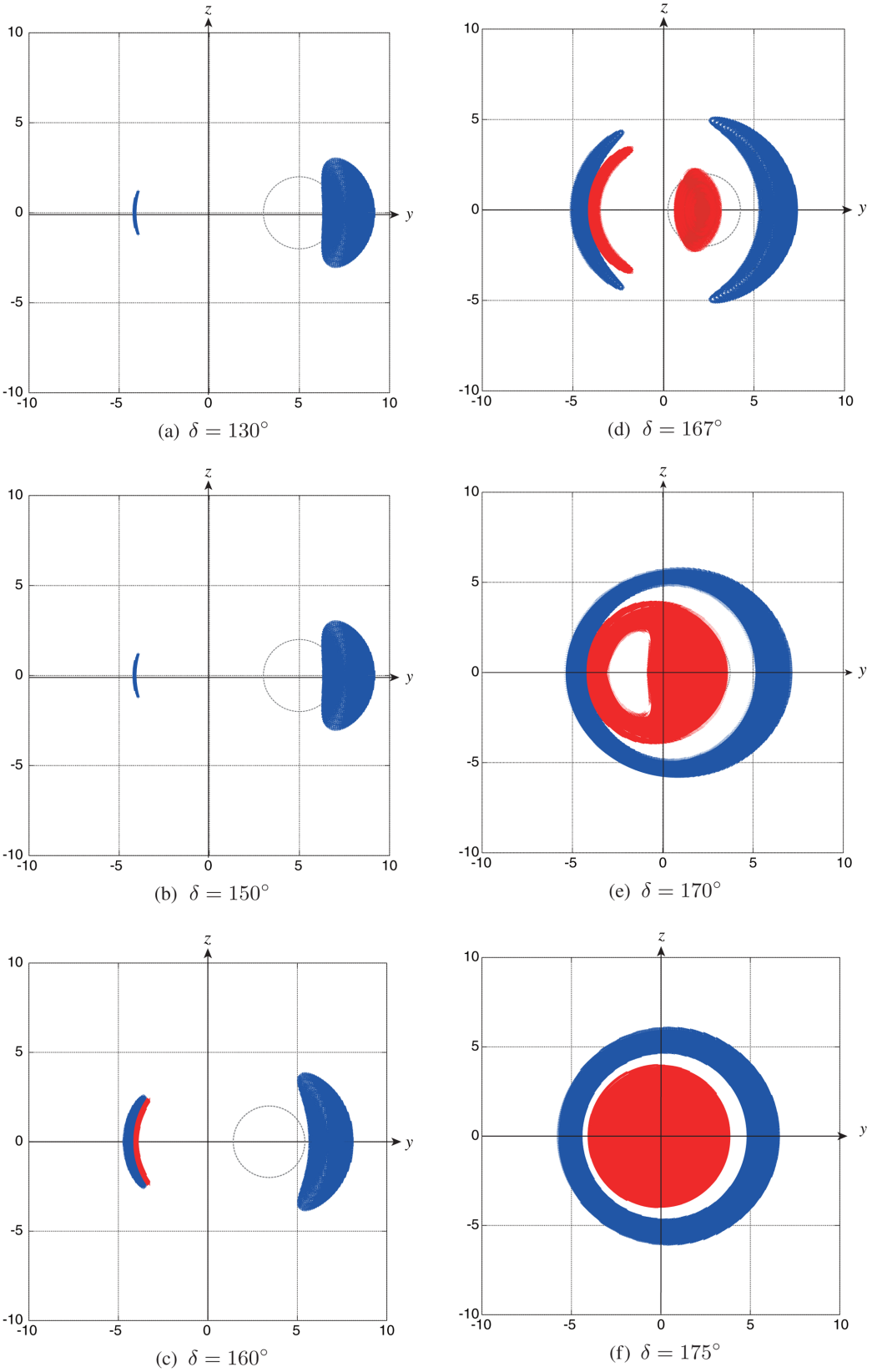

(a) $\delta = 130°$ (d) $\delta = 167°$

(b) $\delta = 150°$ (e) $\delta = 170°$

(c) $\delta = 160°$ (f) $\delta = 175°$

FIG. 10. Images of the companion for Model 2. The gravastar's center is fixed at the origin. Again we choose $D_s = 10r_g$ and $r_s = 2r_g$. We display six snapshots when $\delta = 130°$, 150°, 160°, 167°, 170° and 175° in (a), (b), (c), (d), (e) and (f), respectively. The red images correspond to geodesics which pass through the gravastar, while the blue ones to those which pass only through Schwarzschild background. The dotted circles indicate the image in the absence of the gravastar. We do not take account of light-dark contrast, which is generated by gravitational redshift of the photons.

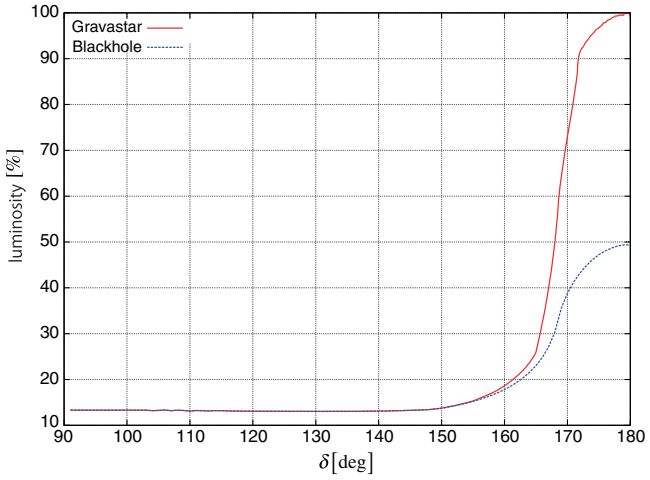

FIG. 11. Light curves for Model 2 gravastar and for the Schwarzschild black hole with the same mass. The ordinate is normalized by the maximum value of the gravastar. We assume that gravitational redshift is negligible; then, the total luminosity is proportional to the apparent area. The maximal luminosity from the gravastar becomes more than twice as large as that from the black hole.

(iii) As δ increases, the two asymmetric red images merge into one. The image when $\delta = 170°$ is in the shape of a disc with a hole.
(iv) When $\delta \gtrapprox 170°$, the area of the inside disc becomes larger than the outer ring. This indicates that the amplification of luminosity by this gravastar is observable.

To see how much the luminosity of the companion is amplified by this gravastar, we plot light curves for Model 2 gravastar and for the Schwarzschild black hole with the same mass in Fig. 11. The ordinate is normalized by the maximum value of the gravastar. We assume that gravitational redshift is negligible; then, the total luminosity is proportional to the apparent area, which is shown in Fig. 10. When $\delta \gtrapprox 160°$, luminosity from the gravastar becomes larger than that from the black hole because photons passing through the gravastar also come to the observer. The maximal luminosity from the gravastar becomes more than twice as large as that from the black hole.

IV. CONCLUDING REMARKS

We have proposed a new method to detect gravastars, by using gravitational lensing effects. We have adopted a spherical thin-shell model of a gravastar developed by Visser and Wiltshire, which connects interior de Sitter geometry and exterior Schwarzschild geometry, and assumed that its surface is optically transparent. We have calculated the image of a companion which rotates around the gravastar; we have found that some characteristic images appear, depending on whether the gravastar possess unstable circular orbits of photons (Model 1) or not (Model 2). For Model 2, we have calculated the total luminosity change, which is called microlensing effects; the maximal luminosity could be so large that the gravastar can be distinguished from the black hole with the same mass.

Finally, we discuss reasonability of our assumption of the optically transparent surface. In the original scenario of gravastars [1], they are assumed to be formed by an unknown phase transition. Therefore, their physical properties are not known, and hence there are three possibilities.

(i) The surface emits electromagnetic waves. In this case one could detect the electromagnetic waves, and hence a gravastar can be distinguished from a black hole observationally.
(ii) The surface is black and does not emit electromagnetic waves. In this case there is no chance to identify a gravastar.
(iii) The surface is electromagnetically transparent.

Because only the last case leads to nontrivial observational consequences, it is worth investigating. Furthermore, if we consider boson stars and other soliton stars composed of scalar fields or gauge fields, they are essentially electromagnetically transparent. Therefore, the present analysis on the assumption of the optically transparent surface is also useful to survey such soliton stars.

[1] P. O. Mazur and E. Mottola, arXiv:gr-qc/0109035; Proc. Natl. Acad. Sci. U.S.A. **101**, 9545 (2004).
[2] C. Cattoen, T. Faber, and M. Visser, Classical Quantum Gravity **22**, 4189 (2005).
[3] A. DeBenedictis, D. Horvat, S. Ilijic, S. Kloster, and K. S. Viswanathan, Classical Quantum Gravity **23**, 2303 (2006); D. Horvat, S. Ilijic, and A. Marunovic, Classical Quantum Gravity **28**, 195008 (2011).
[4] M. Visser and D. L. Wiltshire, Classical Quantum Gravity **21**, 1135 (2004).
[5] P. Rocha, A. Y. Miguelote, R. Chan, M. F. A. da Silva, N. O. Santos, and A. Wang, J. Cosmol. Astropart. Phys. 06 (2008) 025.
[6] B. M. N. Carter, Classical Quantum Gravity **22**, 4551 (2005); D. Horvat and S. Ilijić, Classical Quantum Gravity **24**, 5637 (2007); P. Rocha, R. Chan, M. F. A. da Silva, and A. Wang, J. Cosmol. Astropart. Phys. 11 (2008) 010; R. Chan, M. F. A. da Silva, and P. Rocha, J. Cosmol. Astropart. Phys. 12 (2009) 017; M. E. Gaspar and I. Racz, Classical Quantum Gravity **27**, 185004 (2010); P. Martin-Moruno,

N. M. Garcia, F. S. N. Lobo, and M. Visser, J. Cosmol. Astropart. Phys. 03 (2012) 034; F. S. N. Lobo and R. Garattini, J. High Energy Phys. 12 (2013) 065.

[7] R. Chan, M. F. A. da Silva, J. F. V. da Rocha, and A. Wang, J. Cosmol. Astropart. Phys. 10 (2011) 013.

[8] O. Bertolami and J. Páramos, Phys. Rev. D **72**, 123512 (2005); F. S. N. Lobo, Classical Quantum Gravity **23**, 1525 (2006); N. Bilić, G. B. Tupper, and R. D. Viollier, J. Cosmol. Astropart. Phys. 02 (2006) 013; F. S. N. Lobo, Phys. Rev. D **75**, 024023 (2007); A. DeBenedictis, R. Garattini, and F. S. N. Lobo, Phys. Rev. D **78**, 104003 (2008); R. Chan, M. F. A. da Silva, P. Rocha, and A. Wang, J. Cosmol. Astropart. Phys. 03 (2009) 010; R. Chan, M. F. A. da Silva, and J. F. V. da Rocha, Mod. Phys. Lett. A **24**, 1137 (2009); Gen. Relativ. Gravit. **41**, 1835 (2009); **43**, 2223 (2011); E. Mottola, Acta Phys. Pol. B **41**, 2031 (2010); S. S. Yazadjiev, Phys. Rev. D **83**, 127501 (2011).

[9] F. S. N. Lobo and A. V. B. Arellano, Classical Quantum Gravity **24**, 1069 (2007); D. Horvat, S. Ilijić, and A. Marunović, Classical Quantum Gravity **26**, 025003 (2009); R. Chan and M. F. A. da Silva, J. Cosmol. Astropart. Phys. 07 (2010) 029; A. A. Usmani, F. Rahaman, S. Ray, K. K. Nandi, P. K. F. Kuhfittig, S. A. Rakib., and Z. Hasan, Phys. Lett. B **701**, 388 (2011); C. F. C. Brandt, R. Chan, M. F. A. da Silva, and P. Rocha, J. Mod. Phys. **4**, 869 (2013).

[10] W. Israel, Nuovo Cimento **44B**, 1 (1966).

[11] C. B. M. H. Chirenti and L. Rezzolla, Classical Quantum Gravity **24**, 4191 (2007); Phys. Rev. D **78**, 084011 (2008).

[12] P. Pani, E. Berti, V. Cardoso, Y. Chen, and R. Norte, Phys. Rev. D **80**, 124047 (2009).

[13] A. E. Broderick and R. Narayan, Classical Quantum Gravity **24**, 659 (2007).

[14] T. Harko, Z. Kovaćs, and F. S. N. Lobo, Classical Quantum Gravity **26**, 215006 (2009).

[15] N. Sakai, H. Saida, and T. Tamaki, Phys. Rev. D **90**, 104013 (2014).

[16] V. Cardoso, P. Pani, M. Cadoni, and M. Cavaglia, Phys. Rev. D **77**, 124044 (2008).

[17] S. K. Blau, E. I. Guendelman, and A. H. Guth, Phys. Rev. D **35**, 1747 (1987).